

Numerical study on the rotation capacity of CFRP strengthened cold formed steel beams

Mohammed H. Serror^{*}, Essam G. Soliman^a and Ahmed F. Hassan^b

Department of Structural Engineering, Faculty of Engineering, Cairo University, Egypt

(Received October 24, 2016, Revised January 08, 2017, Accepted January 15, 2017)

Abstract. Currently, CFRP (Carbon Fiber Reinforced Polymer) plate bonding is used quite extensively as a strengthening method. In this technique, a composite CFRP plate or sheet of relatively small thickness is bonded with an adhesion material to steel or concrete structure in order to improve its structural behavior and strength. The sheets or plates do not require much space and give a composite action between the adherents. In this study, the rotation capacity of CFRP-strengthened cold-formed steel (CFS) beams has been evaluated through numerical investigation. Studies on different structural levels have been performed. At the beam level, C-section has been adopted with different values of profile thickness, web height, and flange width. At the connection level, a web bolted moment resistant type of connection using through plate has been adopted. In web-bolted connections without CFRP strengthening, premature web buckling results in early loss of strength. Hence, CFRP sheets and plates with different mechanical properties and geometric configurations have been examined to delay web and flange buckling and to produce relatively high moment strength and rotation capacity. The numerical results reveal that CFRP strengthening may increase strength, initial stiffness, and rotation capacity when compared with the case without strengthening.

Keywords: cold-formed steel beam; rotation capacity; through plate moment connection; carbon fiber reinforced polymer; strengthening

1. Introduction

Cold-formed steel (CFS) sections have several advantages in building constructions, such as the unusual sectional configurations that can be produced economically by cold forming operations, and consequently favorable strength-to-weight ratios can be obtained. Studies have been performed for new profiles such as hat, Z, box and rack sections to predict the appropriate equations that can describe the structural behavior considering the effect of local and distortional buckling (Yu and Schafer 2007, Yang *et al.* 2014, Dinis and Camotim 2015). The use of CFS sections as main structural elements in building constructions is mainly limited to roof purlins and wall girts, mezzanine floors, storage racks and stud-wall frames with low seismic energy dissipation capacity (Lawson 1992, Casafont *et al.* 2006a, b, 2007, Dubina 2008, Moghimi and Ronagh 2009). Generally, moment-resisting frames with CFS sections cannot create plastic hinges in CFS beams; and in turn, cannot produce adequate ductility for high seismic resistance (EC3 2005, AISC 360-10 2010, AISC-341-10 2010, ECP-205 2011). This is attributed to the premature local failures and low strength and stiffness of the CFS beam. The previous studies on behavior of CFS elements and associated beam-column connections in

moment-resisting frames under monotonic and cyclic loading are relatively limited (Casafont *et al.* 2006a, b, 2007, AISI S110 2007, Calderoni *et al.* 2009, Sato and Uang 2009, 2010, Uang *et al.* 2010, Bagheri *et al.* 2012, Phan *et al.* 2013, Dar *et al.* 2015, Padilla-Llano *et al.* 2016). It has been reported that the ductility is mainly provided by the connection (yielding the material around the bolt hole) while the beams and columns remain elastic (Casafont *et al.* 2006a, b, 2007). In recent investigations, conventional back-to-back lipped C-sections possessed a degree of ductile capacity in dissipating seismic energy (Calderoni *et al.* 2009, Bagheri *et al.* 2012, Dar *et al.* 2015); however, they did not satisfy the required width/thickness limits of design codes (EC3 2005, AISC 360-10 2010, AISC 341-10 2010, ECP-205 2011) that aim to delay local buckling after yielding. If CFS beams are used as main dissipative elements in earthquake resistant frame buildings, their ductility needs to be significantly improved by delaying local buckling and allowing development of large plastic deformations. This can be achieved by optimizing the shapes of the CFS sections, using pertinent connection details, employing out-of-plane stiffeners, and strengthening the section profile with CFRP (Wong and Chung 2002, Lim and Nethercot 2003, Yu *et al.* 2005, Dar *et al.* 2015, Serror *et al.* 2016, Hassan *et al.* 2017). The favorable mechanical properties of fiber reinforced polymer (FRP) composites include high strength, corrosion resistance, and ease of application. Carbon fiber reinforced polymer (CFRP) composites are the widely used FRP composites with respect to strengthening of steel structures (Sayed-Ahmed 2004, Zhao and Zhang 2007, Silvestre *et al.*

*Corresponding author, Associate Professor,
E-mail: serror@eng.cu.edu.eg

^a Graduate Student

^b Professor

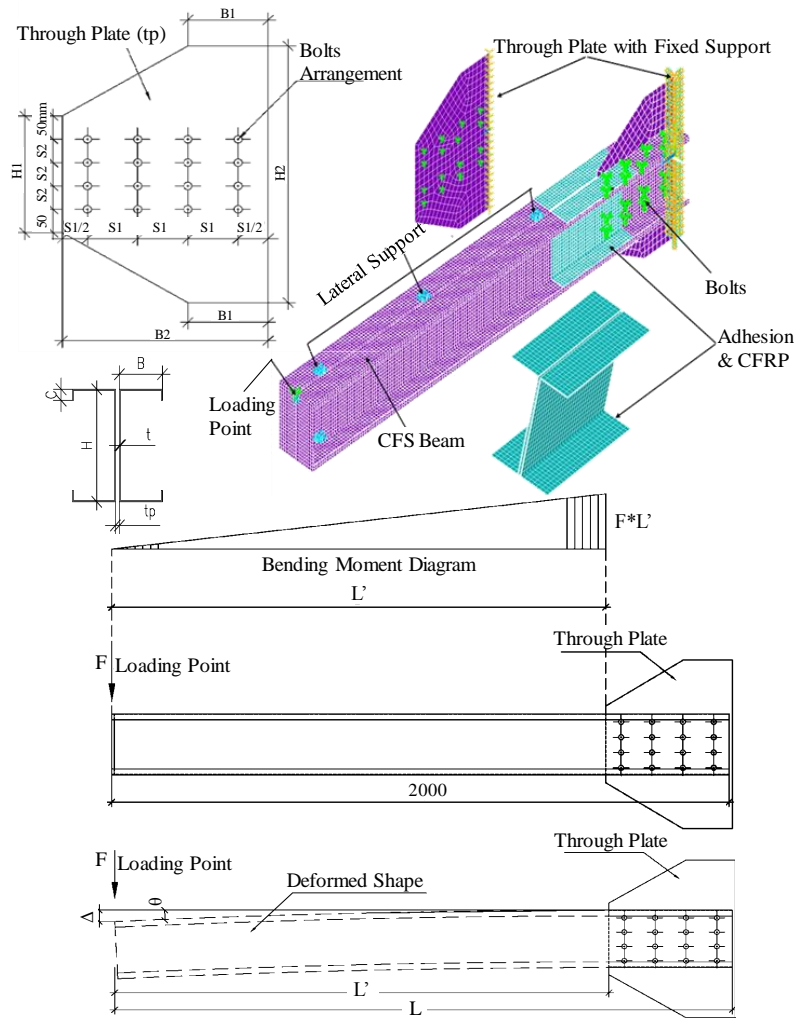


Fig. 1 Numerical model parameters and boundary conditions

2008, Linghoff *et al.* 2009). Compared with the conventional technique of welding steel plates and stiffeners, the application of CFRP composites avoids the procedure of welding and the occurrence of residual stresses. Furthermore, welding steel plates and stiffeners to thin-walled profiles of cold-formed steel requires special consideration in workmanship, and in turn, imposes more fabrication effort. In addition, the utilization of steel plates and stiffeners inversely affects the favorable strength-to-weight ratio of CFS members. Hence, the CFRP plate or sheet bonding is used to enhance the behavior of structural steel elements against instability, improving both strength and ductility (Zhao and Al-Mahaidi 2009, Harries *et al.* 2009, El-Tawil *et al.* 2011, Faris and Mehtab 2013, Islam and Young 2014, Park and Yoo 2015, Gunaydin *et al.* 2015, Gholami *et al.* 2016). It is worth noting that the previous studies are considered relatively limited.

This paper presents a numerical prediction of available rotation capacity of CFRP-strengthened CFS beams. This is in continuation of the numerical and experimental studies performed by the authors (Serror *et al.* 2016, Hassan *et al.* 2017). It is worth noting that the investigation of the beam-to-column connection is considered beyond the scope of study at this stage. A web bolted to through plate connection

has been adopted, assuming rigid support for the column and full node coupling at bolt location, as shown in Fig. 1.

2. Numerical model

As shown in Fig. 1, the numerical FE model has been established, in ANSYS (1998), for 2 m long CFS beams to evaluate the rotation capacity. A web bolted to through-plate connection has been adopted, where the column is substituted with restrained boundary conditions (rigid column). The boundary conditions, loading points and constraints are shown in Fig. 1. For the CFS beam, the parameters of the FE model are: element type: 4-node shell element (shell181), mesh size: 12.5 mm \times 12.5 mm, and material: bi-linear stress-strain behavior (DIN-17100 ST-37) with $F_y = 240$ MPa (yield stress), $F_u = 360$ MPa (tensile stress), $E = 210$ GPa, (elasticity modulus), $E_s = E/100$ (hardening modulus) and $\nu = 0.33$ (Poisson's ratio). In correspondence with the geometric parameters indicated in Fig. 1, the dimensions of CFS beams and associated through plates are listed in Table 1. The FE models have been generated to cover the adopted range of parameters including various dimensions of the through plate and the

Table 1 Adopted parameters and range of study of CFS beams

Web depth (H , mm)	120	150	200	250	300	350	400
Flange width (B , mm)	65		85		100		
Flange lip (C , mm)	15		20		25		
Beam length (L , mm)	2000						
Thickness (t , mm)	1.5, 2, 2.5 and 3 for each beam profile						

Table 2 CFRP material properties as given by the manufacture (SIKA 2016)

CFRP	Thickness (t , mm)	Ultimate tensile strength (σ_u , MPa)	Tensile E-modulus (E_o , GPa)	Strain at peak (ϵ_{fs} , %)
Sika CarboDur S1214 (Laminate Plate)	1.400	3100	165	1.7
SikaWarp-230c (woven sheet)	0.131	4300	238	1.8
SikaWarp-300c (woven sheet)	0.170	3900	230	1.5
SikaWarp-301c (woven sheet)	0.170	4900	230	2.1

CFS beam. For the CFRP plate or sheet, the parameters of the FE model are: element type: 8-node solid element (SOLID185), mesh size: 12.5 mm \times 12.5 mm, and material: linear orthotropic stress-strain behavior with mechanical properties as per manufacture (SIKA 2016) and as listed in Table 2. For the adhesion material, the parameters of the FE model are: element type: 8-node solid element (SOLID185), mesh size: 12.5 mm \times 12.5 mm, and material: linear

Table 3 Adhesion material properties as given by the manufacture (SIKA 2016)

Adhesion material	Thickness (t , mm)	Ultimate tensile strength (σ_u , MPa)	Tensile E-modulus (E_o , GPa)	Strain at peak (ϵ_{fs} , %)
Sikadur-30: for Laminate Plate	1.0	24.8	4.482	1.0
Sikadur-300: for Woven Sheet	0.25	55	1.724	3.0

isotropic stress-strain behavior with mechanical properties as per manufacture (SIKA 2016) and as listed in Table 3. The adopted FE mesh size has been selected upon mesh sensitivity analysis. Meanwhile, the CFS beam, the adhesion material and the CFRP plate or sheet are all considered in full interfacial bond. Furthermore, initial imperfection has been adopted in compliance with the fundamental buckling mode shape attaining maximum amplitude of [beam height/10,000]. Hence, nonlinear inelastic post-buckling analysis has been performed. The FE model has been established to be as simple as possible, where the bolts that connect the CFS beam with the through plate have been modeled as point ties. Because of this simplification, the tied points, replacing the bolts, do not allow uniform rotation of the bolt group. This simplification is on the conservative side since the critical demand is on the beam and the FE model increases this demand slightly. It is worth noting that the FE model has been designed to enable inelastic behavior in the beam, while the through plate remains elastic. Furthermore, the connector between the beam back-to-back elements has been modeled using rigid beam element (MPC184). The loading point has been selected at the end of the beam, where a pair of vertical stiffeners has been employed to prevent the local failure.

Different values of beam profile thickness have been adopted in the range from 1.5 mm up to 3 mm. The width/thickness ratios of the compression elements of steel sections are restricted by design codes to certain limits to

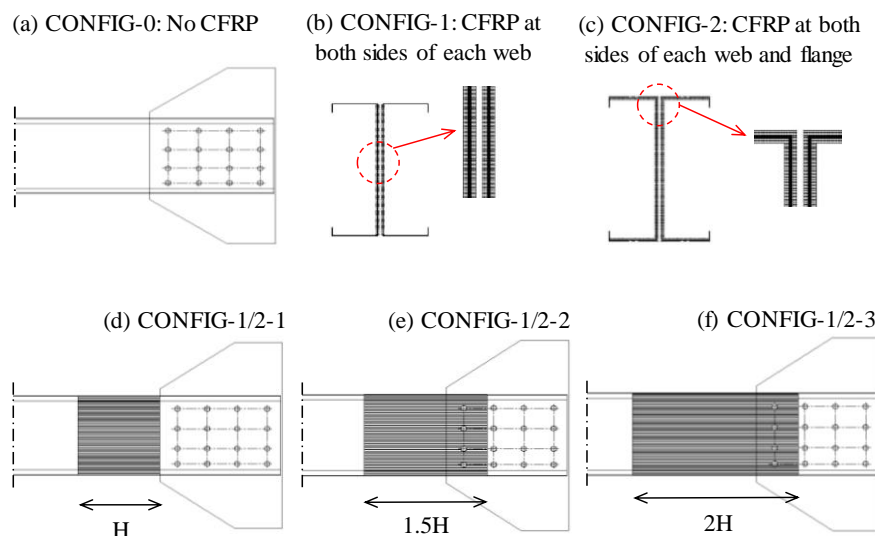


Fig. 2 CFRP-strengthening configurations

avoid local buckling before yielding. These width/thickness ratio limits are not possible to be satisfied by typical CFS sections. Local buckling of CFS sections, however, can be delayed by strengthening with CFRP plate or sheet, rather than restricting the width/thickness ratio.

The web bolted to through-plate connection suffers premature web buckling in the beam. To mitigate this loss of strength, one approach is to employ out-of-plane stiffeners. However, as reported in the literature, welding of stiffeners to thin-walled profiles requires special consideration in workmanship, and in turn, imposes more fabrication effort. In addition, the utilization of out-of-plane stiffeners inversely affects the favorable strength-to-weight ratio of CFS members (Serror *et al.* 2016, Hassan *et al.* 2017).

Therefore, the approach adopted in this study is to delay the premature web buckling of the beam by employing CFRP sheets or plates. This, in turn, enhances the CFS beam rotation capacity.

Three different configurations of CFRP-strengthening have been examined as shown in Fig. 2. CONFIG-0 represents the set of models without strengthening, as shown in Fig. 2(a). CONFIG-1 represents the set of models strengthened with CFRP at the two sides of beam webs, as shown in Fig. 2(b). CONFIG-2 represents the set of models strengthened with CFRP at both sides of the two webs and the four flanges of the beam, as shown in Fig. 2(c). Each of CONFIG-1 and CONFIG-2 consists of three subgroups: CONFIG-1/2-1, CONFIG-1/2-2 and CONFIG-1/2-3 based on the length of CFRP that is equal to H, 1.5 H and 2H, respectively, as shown in Figs. 2(d), (e) and (f). The CFRP of length H is extended from the end of the through plate towards the opposite side of the connection for a distance equal to the beam height (H). The CFRP of length 1.5 H is similar to that of length H plus an extension of 0.5 H towards the connection side, i.e., covering the first row of bolts. The CFRP of length 2 H is similar to that of 1.5 H plus an extension of 0.5 H towards the opposite side of the connection. Furthermore, five suffix letters from “A” to “E” are attached to the geometric configuration tag in order to distinguish five different sets of CFRP and associated adhesion material from the list of Tables 2 and 3 (i.e., CONFIG-1-1-A is of geometric configuration group CONFIG-1-1 applying CFRP of set “A”). The set “A” represents one layer of adhesion Sikadur-30 plus one layer of CFRP plate Sika CarboDur-S1214. The set “B” represents one layer of adhesion Sikadur-300 plus one layer of CFRP sheet SikaWarp-230c. The set “C” represents two layers of adhesion Sikadur-300 plus two layers of CFRP sheet SikaWarp-230c. The set “D” represents one layer of adhesion Sikadur-300 plus one layer of CFRP sheet SikaWarp-300c. The set “E” represents one layer of adhesion Sikadur-300 plus one layer of CFRP sheet SikaWarp-301c.

Monotonic loading has been applied to the FE models at a constant rate of 0.1 mm/sub-step. Meanwhile, a maximum value of 0.05 rad. has been adopted as upper boundary for the rotation angle. For the definition of beam maximum moment, M, and rotation angle, θ , the middle section of the plastic hinge region of the beam is assumed to be at the end of the through plate, as shown in Fig. 1. Hence, the rotation angle can be calculated as $[\theta = \Delta / L']$. Fig. 1 shows the

definition of displacement (Δ), rotation angle (θ) and effective length of beam to the end of through plate (L'). The rotation angle associated with the maximum attained bending moment is defined as the rotation capacity. The numerical results obtained in this study have been verified against experimental investigations in the literature (Islam and Young 2014, Serror *et al.* 2016).

3. Results and discussion

3.1 Numerical model verification

The numerical parameters employed in this study (element types, mesh size, and material models) have been verified against numerical and experimental models in the literature. The CFS beam model, without strengthening, has been verified against beam specimen that has been tested under monotonic loading by the authors within experimental investigation associated with this numerical study (Serror *et al.* 2016). Table 4 lists the characteristics of the verification specimen. The details of the experiment setup, as shown in Fig. 3(a), have been provided in the experimental study (Serror *et al.* 2016), including supporting system; loading system; specimen and instrumentations. Fig. 3(b) shows the numerical results of specimen rotation capacity in comparison with the experimental ones. Apparently, the results are in good match, in terms of initial stiffness (elastic stiffness) and rotation capacity. Furthermore, it has been reported (Serror *et al.* 2016, Hassan *et al.* 2017) that both results are also in good match in terms of location and mode of instability and location of maximum stresses. In addition, the CFS beam model, without strengthening, has been verified against Bagheri *et al.* (2012) numerical model of CFS C-section (200×100×25/3) under monotonic loading. It has been reported by the authors that the rotation capacity results of both models are in good agreement (Hassan *et al.* 2017).

On the other hand, the strengthening model with CFRP bonding, including adhesion material, has been verified against Islam and Young (2014) experimental and numerical models. The model has been generated for a CFS specimen with a length equal to 350 mm and a hollow rectangular section with depth equal to 100 mm, width equal to 50 mm, and thickness equal to 2.5 mm. The specimen has been strengthened at the mid-span with CFRP plate with properties of: 50 mm length, 3100 MPa ultimate tensile strength, 165 GPa elasticity modulus, and 1.4mm thickness, as shown in Fig. 3(c). The adhesion material has been applied with properties of: 24.3 MPa ultimate tensile stress, 1.6 GPa elasticity modulus, and 1.0 mm thickness.

Table 4 Test specimen used for numerical model verification (Serror *et al.* 2016)

Specimen ID	CFS Beam		Through Plate		Loading scheme
	Beam section shape	Dimensions (mm) H×B×C/t	Dimensions (mm) (H2/H1×B2/B1)	t_p (mm)	
B03	C	300×100×25/3	650/350×450/175	10	Monotonic

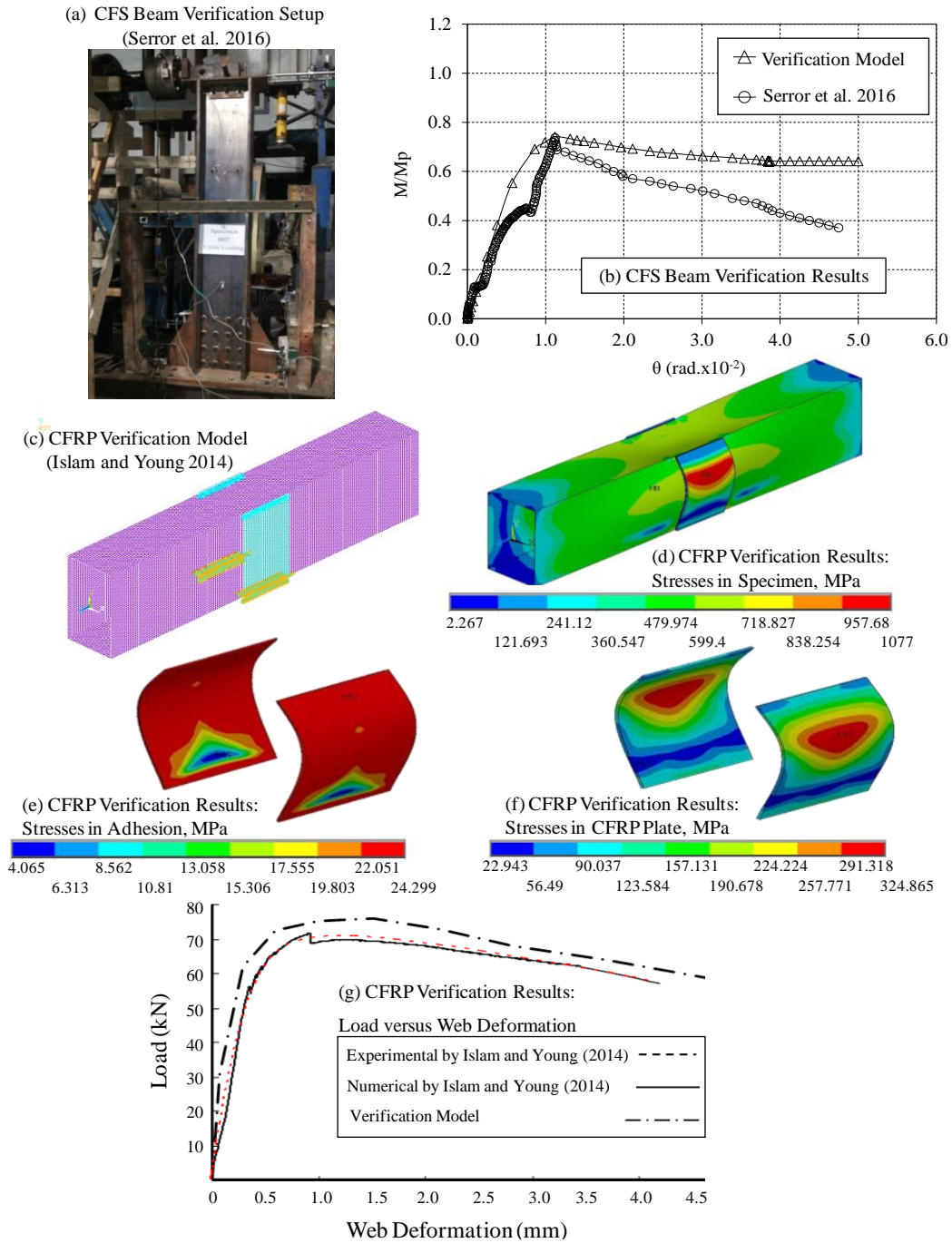


Fig. 3 Numerical model verification results

Monotonic loading has been applied at the mid-span, where failure has been observed in the adhesion material. Figs. 3(d), (e) and (f) demonstrate Von-Misses stresses as resulted in the specimen, the adhesion material, and the CFRP plate, respectively. It is evident that the onset of failure is emerged in the adhesion material, in compliance with the experimental observation, where stresses are attaining the ultimate limit. Fig. 3(g) reports the load-web deformation results of the verification model against both numerical and experimental results of Islam and Young (2014). It is evident that the results are in good agreement. It is also sound that the CFRP-strengthened CFS section has enhanced load capacity and delayed premature buckling. It is worth noting that the

differences between the experimental results and the numerical predictions can be attributed to: imperfections; differences between material properties of test specimen and numerical model; actual dimensions of test specimens; and residual stresses. These factors were not taken into account by the numerical analysis at this stage.

3.2 CFRP strengthening results

Fig. 4 demonstrates the resulted premature buckling in absence of CFRP strengthening, CONFIG-0. It is evident that there are particular locations susceptible to premature buckling (Serror *et al.* 2016, Hassan *et al.* 2017) at: end of

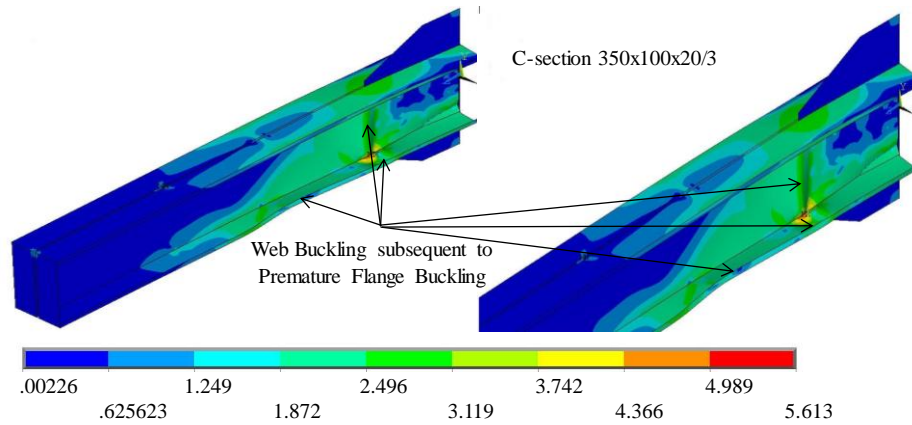


Fig. 4 Premature buckling in absence of CFRP strengthening (CONFIG-0), with Von-Misses stress distribution in $MPa \times 10^2$

the through plate (nearby the first row of bolts), and the web-to-through plate connection. This observation highlights the positions where CFRP strengthening is indicated. Two different CFRP strengthening configurations have been examined as explained in Section 2 and as shown in Fig. 2, namely: CONFIG-1 and CONFIG-2, where CONFIG-0 represents the non-strengthened case. The FE results of the beam normalized bending moment (M/Mp) versus rotation angle (θ) have been illustrated, for selected beams, in Figs. 5 and 6 applying all CFRP-strengthening configurations. Meanwhile, Figs. 7 and 8 report the resulted failure mode in association with each configuration, for the same set of selected beam models. Table 5 lists the maximum attained bending moment and the associated rotation capacity for the selected beam models, with respect to each strengthening configuration. Moreover, Figs. 9 and 10 demonstrate the failure mode in association with the deformed shape and Von-Misses stress distribution. The results for the full range of parameters have been reported in the reference (Essam *et al.* 2016).

It is evident in Figs. 5 and 6 that the beams without strengthening (CONFIG-0) showed the lowest strength, rotation capacity and initial stiffness compared with beams employing CFRP strengthening. Extending the CFRP to cover the first row of bolts (CONFIG-1-2 and CONFIG-2-2) did afford significant increase in strength, rotation capacity and initial stiffness compared with the case where CFRP stops at the end of the through plate (CONFIG-1-1 and CONFIG-2-1). This is apparent when comparing Figs. 5(bii) and 6(bii) with Figs. 5(bi) and 6(bi), respectively. Meanwhile, extending the CFRP further away from the through plate connection (CONFIG-1-3 and CONFIG-2-3) did not afford any significant addition to the behavior reported with CONFIG-1-2 and CONFIG-2-2. This is apparent when comparing Figs. 5(biii) and 6(biii) with Figs. 5(bii) and 6(bii), respectively. This conclusion is further revealed in Figs. 7(b) and 8(b). CONFIG-1-3 and CONFIG-2-3 did not add significant increase to CONFIG-1-2 and CONFIG-2-2 in terms of beam strength, and further did not change the reported failure modes. Contrarily, CONFIG-1-2 and CONFIG-2-2 did afford significant increase in beam strength and did change the failure modes reported with CONFIG-1-1 and CONFIG-2-1, where the steel premature buckling failure modes have been changed to failure in

Table 5 Maximum attained bending moment and associated rotation capacity for selected beam models

		Beam 300×100×20/1.5			Beam 350×100×20/3.0		
	CFRP configuration	M_{max} / Mp	θ at M_{max} (rad.* 10^{-2})		M_{max} / Mp	θ at M_{max} (rad.* 10^{-2})	
	CONFIG-0	0.45	0.55	CONFIG-0	0.70	0.94	
CONFIG-1-1	A	0.57	0.66	CONFIG-1-1	A	0.77	1.46
	B	0.52	0.68		B	0.72	1.05
	C	0.53	0.69		C	0.72	1.07
	D	0.51	0.67		D	0.72	1.03
	E	0.52	0.67		E	0.72	1.02
CONFIG-1-2	A	0.78	0.68	CONFIG-1-2	A	1.20	3.02
	B	0.68	0.72		B	0.93	2.12
	C	0.72	0.74		C	1.10	3.40
	D	0.68	0.74		D	0.92	2.14
	E	0.69	0.74		E	0.92	2.14
CONFIG-1-3	A	0.92	1.01	CONFIG-1-3	A	1.25	4.35
	B	0.80	1.02		B	0.93	2.12
	C	0.84	1.03		C	1.10	3.04
	D	0.81	1.05		D	0.93	2.14
	E	0.82	1.10		E	0.93	2.14
CONFIG-2-1	A	0.58	0.66	CONFIG-2-1	A	0.78	1.24
	B	0.58	0.70		B	0.73	1.03
	C	0.56	0.72		C	0.73	1.09
	D	0.57	0.72		D	0.73	1.03
	E	0.57	0.72		E	0.73	1.02
CONFIG-2-2	A	0.82	0.68	CONFIG-2-2	A	1.24	2.73
	B	0.69	0.72		B	1.08	2.37
	C	0.73	0.79		C	1.16	2.01
	D	0.69	0.75		D	1.07	2.54
	E	0.69	0.75		E	1.08	2.44
CONFIG-2-3	A	0.84	0.90	CONFIG-2-3	A	1.50	4.38
	B	0.83	0.92		B	1.13	3.20
	C	0.87	0.94		C	1.30	3.01
	D	0.83	0.95		D	1.13	3.25
	E	0.83	0.95		E	1.13	3.25

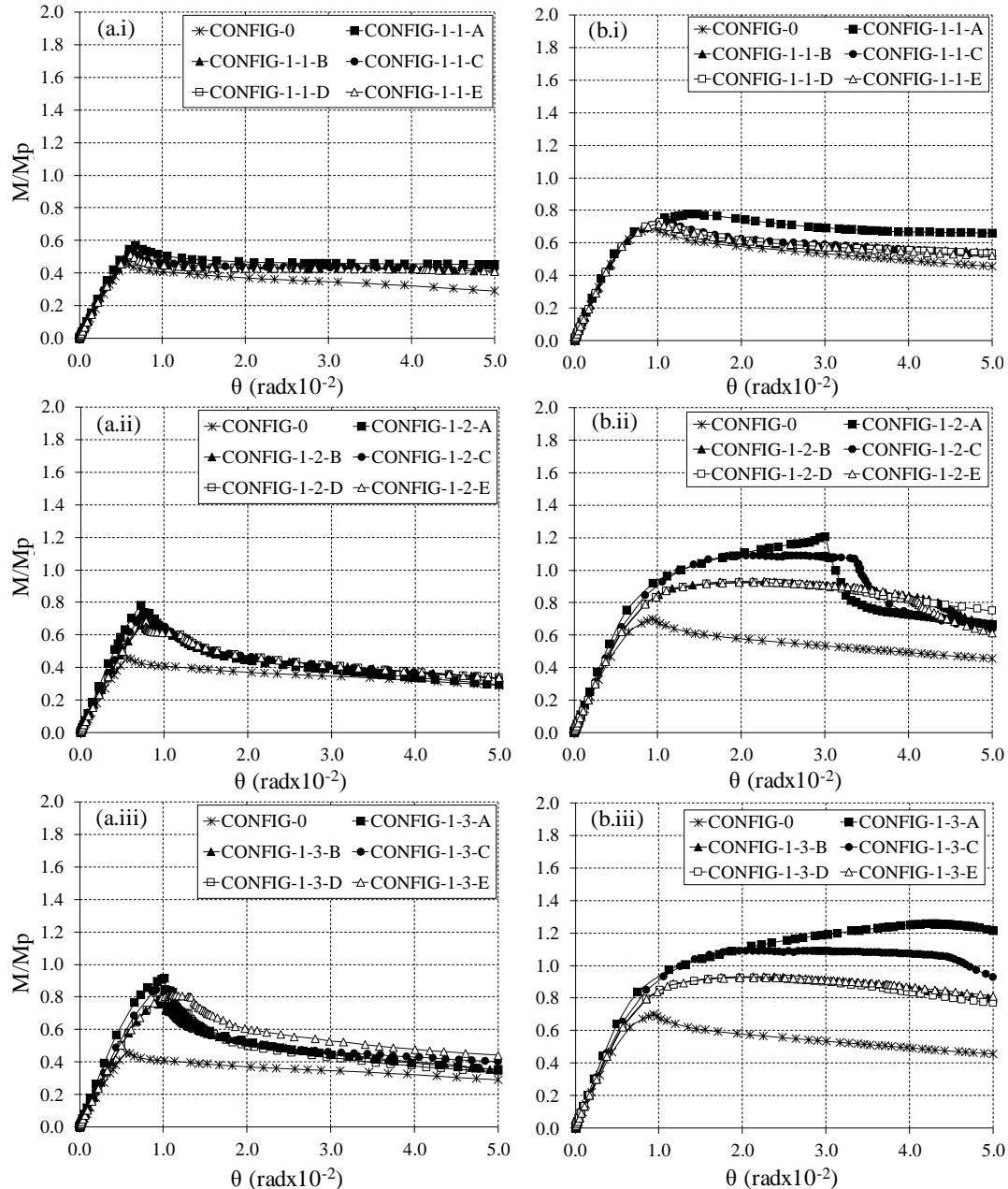


Fig. 5 Normalized moment (M/M_p) versus rotation angle (θ) for: (a) Beam with section $300 \times 100 \times 20/1.5$; and (b) Beam with section $350 \times 100 \times 20/3$, with CFRP strengthening in CONFIG-1

adhesion and CFRP.

Furthermore, the results revealed that strengthening the beam flanges in addition to the webs (CONFIG-2) did not afford significant increase in terms of strength, initial stiffness and rotation capacity compared with the case where strengthening is applied only to the webs (CONFIG-1). This is attributed to the fact that the adopted connection is “web bolted to through plate”, where the loads/stresses are transferred from the beam flanges to the web at the connection. Consequently, the web strengthening has much more influence on the beam behavior compared with the flange strengthening. This is the essence behind the reported insignificant increase when changing CONFIG-1 to CONFIG-2, as reported in Figs. 5 and 7 compared with Figs. 6 and 8. It is worth noting that the assessment of the

reported increase as “insignificant” is in fact relative to the additional cost and workmanship that are needed to change CONFIG-1 to CONFIG-2.

Upon the obtained results, it is apparent that the utilization of CFRP strengthening is considered more effective with beams that have lower web slenderness ratio ($H/t < 200$), when compared with those having higher slenderness ($H/t \geq 200$). It is worth noting that this slenderness limit is inferred based on the range of the studied parameters and still higher than that specified in the design codes. The effectiveness of CFRP strengthening in terms of strength, initial stiffness and rotation capacity can be explained when comparing Figs. 5(a), 6(a), 7(a) and 8(a) of beam with section ($300 \times 100 \times 20/1.5$) with Figs. 5(b), 6(b), 7(b) and 8(b) of beam with section ($350 \times 100 \times 20/3$),

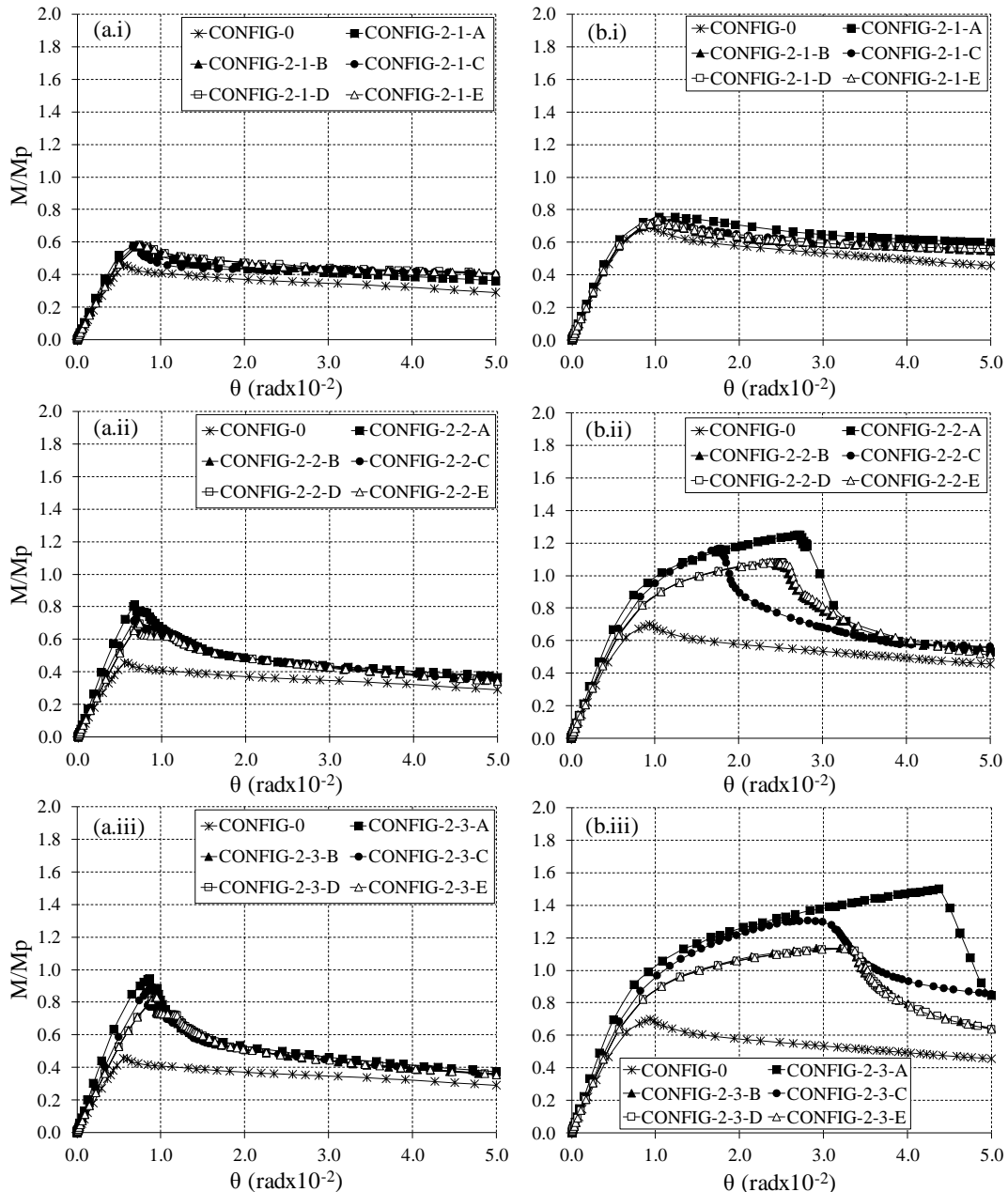


Fig. 6 Normalized moment (M/M_p) versus rotation angle (θ) for: (a) Beam with section $300 \times 100 \times 20/1.5$; and (b) Beam with section $350 \times 100 \times 20/3$, with CFRP strengthening in CONFIG-2

respectively. The beam with section ($300 \times 100 \times 20/1.5$, $H/t = 200$) could attain a moment capacity of more than $0.8 M_p$ at a rotation capacity of more than $0.9E-2$ rad by employing CFRP of CONFIG-1-3 or CONFIG-2-3 with any CFRP set of "A to E". On the other hand, the beam with section ($350 \times 100 \times 20/3$, $H/t = 116.7$) could attain a moment capacity of more than $1.0 M_p$ at a rotation capacity of more than 0.02 rad by employing CFRP of CONFIG-1-2-A/C, CONFIG-1-3-A/C, CONFIG-2-2-A to E, or CONFIG-2-3-A to E. Meanwhile, the same beam can attain a moment capacity of more than $0.9 M_p$ at a rotation capacity of more than 0.02 rad. by employing CFRP of CONFIG-1-2-B or CONFIG-1-3-B.

Figs. 7(a) and 8(a) demonstrate that the steel failure mode is dominating over the adhesion/CFRP failure mode

for the beam with section ($300 \times 100 \times 20/1.5$, $H/t = 200$), reflecting the marginal contribution of CFRP strengthening. Contrarily, Figs. 7(b) and 8(b) demonstrate that the adhesion/CFRP failure mode is dominating over the steel failure mode for the beam with section ($350 \times 100 \times 20/3$, $H/t = 116.7$), reflecting the valuable contribution of CFRP strengthening. It is evident as well that doubling the number of the employed CFRP sheets (set-C versus set-B) affords insignificant addition to the behavior resulted with the single layer strengthening, considering the needed additional cost and workmanship.

Moreover, it is apparent that the CFRP strengthening with set B, D or E reveals almost the same behavior with insignificant difference. This is attributed to the fact that the failure has been observed in the adhesion material, which is

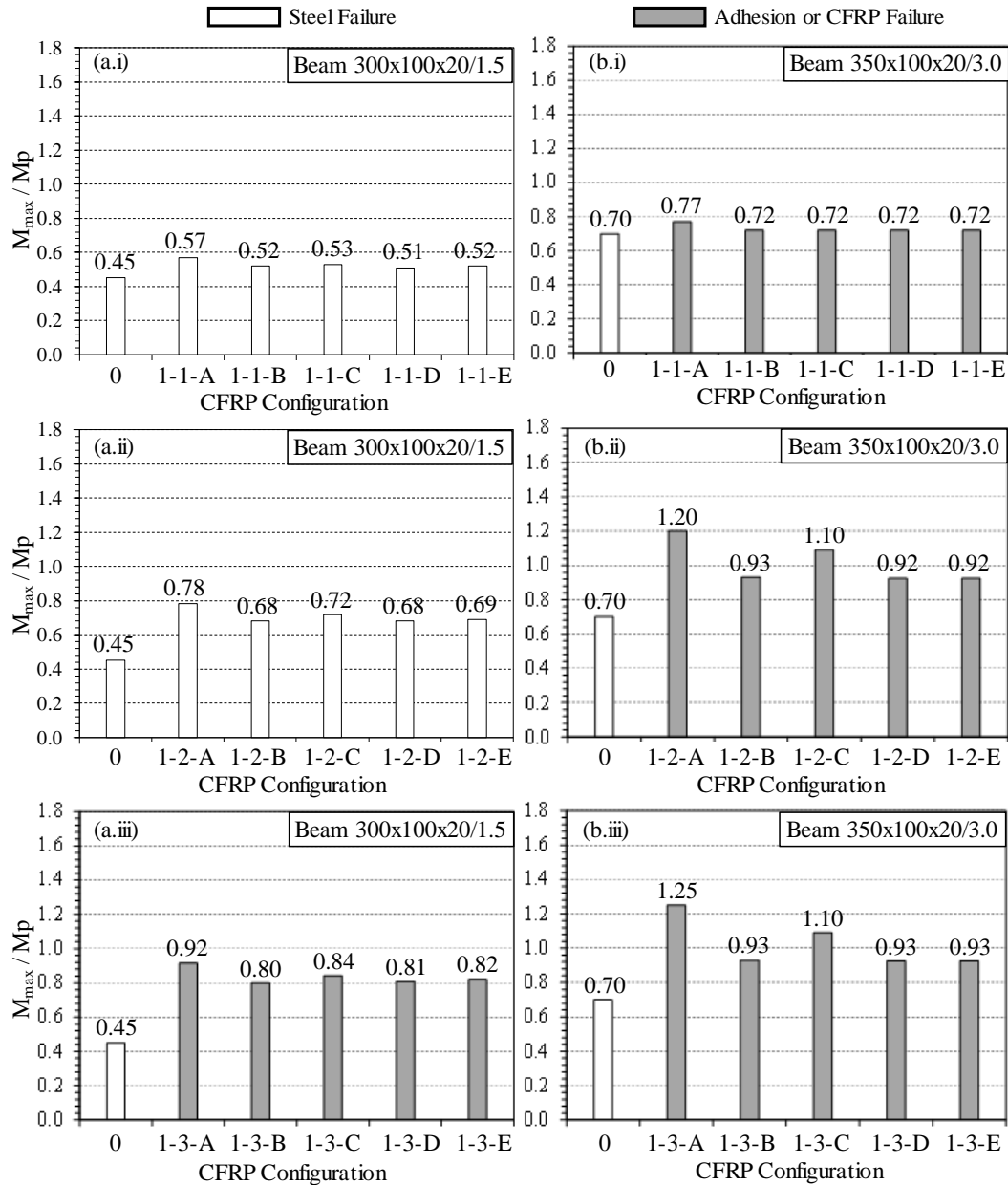


Fig. 7 The maximum attained moment and the associated failure mode for: (a) Beam with section 300×100×20/1.5; and (b) Beam with section 350×100×20/3, with CFRP strengthening in CONFIG-1

identical for the three sets of CFRP sheets as per the manufacture (SIKA 2016). It is worth noting that the contact interfaces between steel, adhesion material and CFRP sheet/plate require further study with various mechanical properties of the adhesion material. The aforementioned observations are further explained in Figs. 9 and 10, for CONFIG-1 and CONFIG-2 respectively.

Fig. 9 demonstrates Von Misses stress distribution along with the premature buckling as resulting in the beam with section (350×100×20/3), employing CONFIG-1-2-A and CONFIG-1-2-B. It is evident that the position of maximum stresses is located at the end of the through plate, where the loads are transferred from the web to the through plate. It is also evident that the premature buckling is delayed and shifted away from the strengthened part of the beam. Fig. 10 demonstrates Von Misses stress distribution along with

the premature buckling as resulting in the beam with section (350×100×20/3), employing CONFIG-2-1-A and CONFIG-2-1-B. Similarly, the position of maximum stresses is located at the end of the through plate. However, in comparison with Fig. 4 of CONFIG-0, it is apparent that the CFRP has a marginal contribution. The premature buckling is not delayed and not shifted away from the strengthened part of the beam. This is attributed to the fact that the CFRP configuration is not covering the first row of bolts within the through plate connection.

Hence, CONFIG-1-2-A and CONFIG-1-2-B can be recommended for CFRP plate and sheet bonding, respectively, over the other configurations, while affording higher rotation capacity and utilizing effective volume of CFRP strengthening.

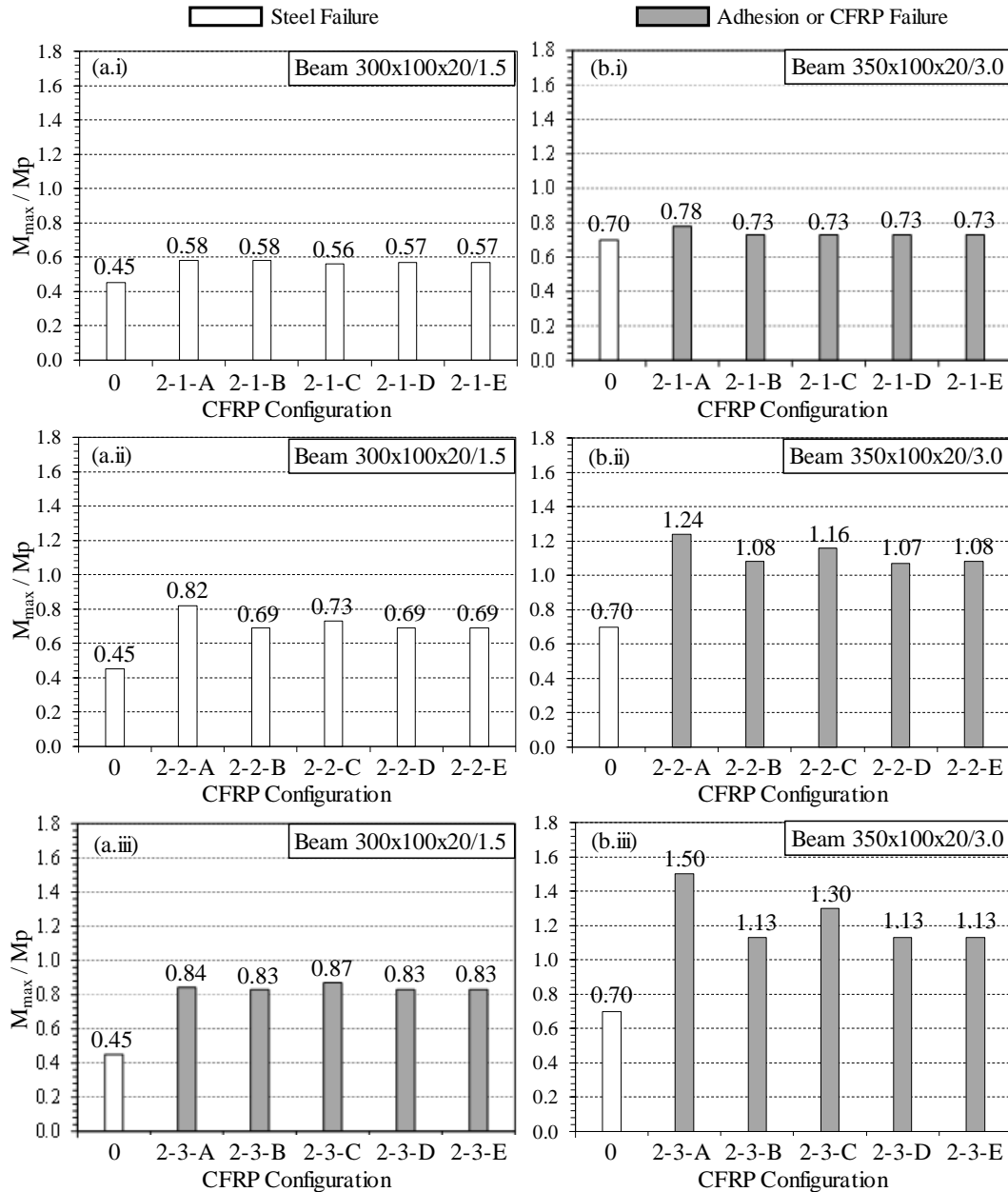


Fig. 8 The maximum attained moment and the associated failure mode for: (a) Beam with section $300 \times 100 \times 20 / 1.5$; and (b) Beam with section $350 \times 100 \times 20 / 3$, with CFRP strengthening in CONFIG-2

4. Conclusions

In this study, a numerical investigation has been presented to underpin the usage of cold-formed steel (CFS) beams as structural elements. Three-dimensional nonlinear FE models have been established for CFS beams with web bolted to through plate connection. CFRP sheet/plate bonding has been applied and examined to strengthen the beam under monotonic loading, where the rotation capacity has been evaluated. The CFRP strengthening has been tested with different geometric configurations and mechanical properties. The main conclusions, within the range of the studied models and parameters, can be summarized as follows:

(1) The studied CFS beams could achieve a strength

ranging from 0.20 Mp up to almost 1.0 Mp without employing CFRP strengthening.

- (2) The premature buckling is delayed when CFRP sheet/plate is applied with a configuration that covers, at least, the first row of bolts in the through plate connection. Consequently, the beam initial stiffness, strength and rotation capacity are increased. Furthermore, this configuration enables the plastic hinge to be formed away from the connection.
- (3) The CFS beams with web slenderness ratio less than 200 can attain a moment capacity of more than 0.9 Mp at a rotation capacity of more than 0.02 rad by employing CFRP strengthening of particularly designed configurations (CONFIG-1-2-A or CONFIG-1-2-B).

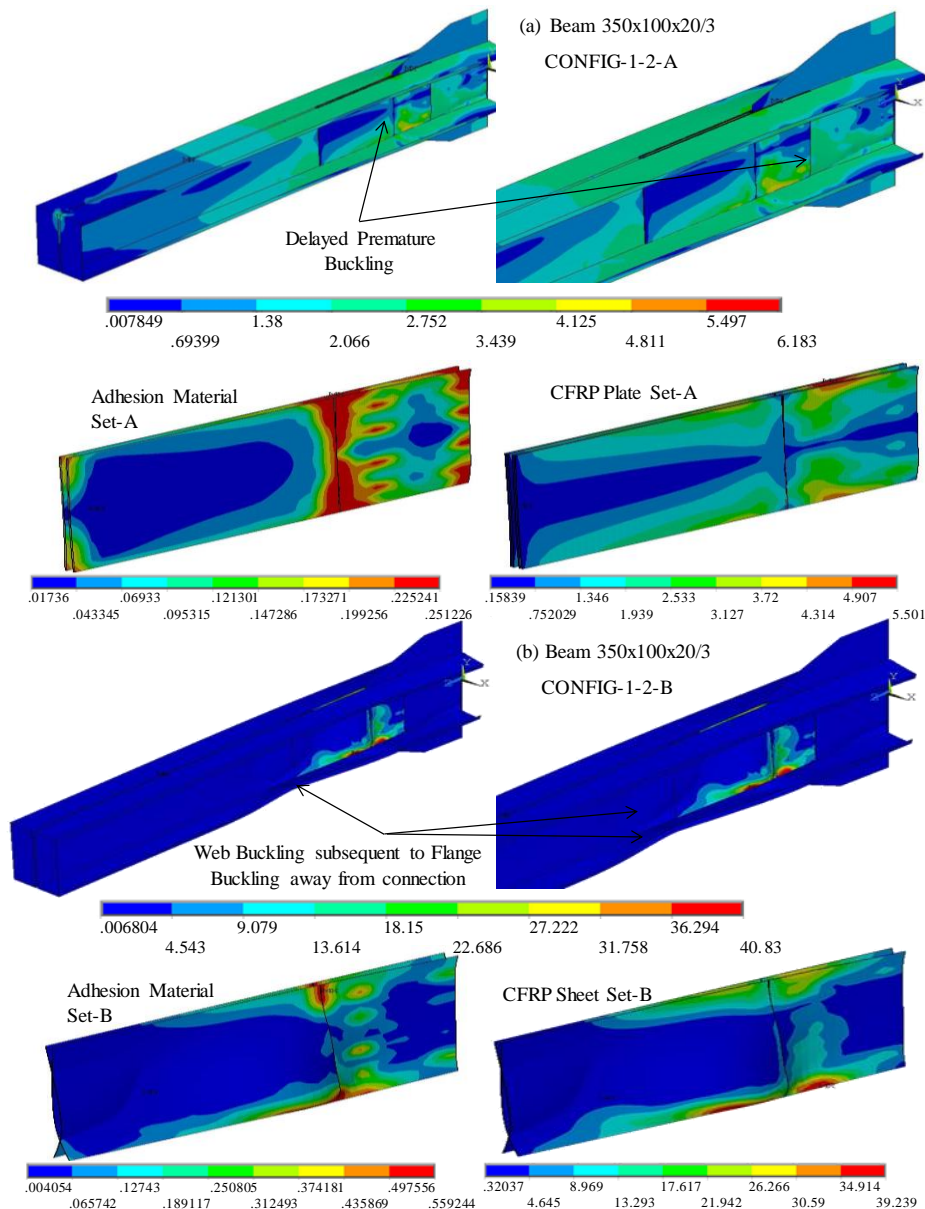


Fig. 9 Premature buckling upon utilization of CFRP strengthening: (a) CONFIG-1-2-A; and (b) CONFIG-1-2-B, with Von-Mises stress distribution in $\text{MPa} \times 10^2$

- (4) The CFS beams with web slenderness ratio more than or equal to 200 can attain a moment capacity of more than 0.8 Mp at a rotation capacity of more than 0.01 rad by employing CFRP strengthening of particularly designed configurations (CONFIG-1-3 with any CFRP set of “A to E”).
- (5) Doubling the number of CFRP sheets (set-C versus set-B) affords insignificant addition to the behavior resulted with the single layer strengthening, considering the needed additional cost and workmanship.
- (6) Strengthening the beam flanges in addition to the webs (CONFIG-2) did not afford significant increase in terms of strength, initial stiffness and rotation capacity, compared with the case where strengthening is applied only to the webs (CONFIG-1). This is attributed to the adopted web bolted to

through plate connection, where the loads/stresses are transferred from the beam flanges to the web at the connection.

- (7) Enhancing the mechanical properties of the CFRP sheet/plate requires a relevant enhancement for the mechanical properties of the associated adhesion material, for effective contribution.

Acknowledgments

The authors would like to express their gratitude to Cairo University, Faculty of Engineering, for funding the experimental testing associated with this numerical study.

References

AISI S110 (2007), Standard for Seismic Design of Cold-Formed

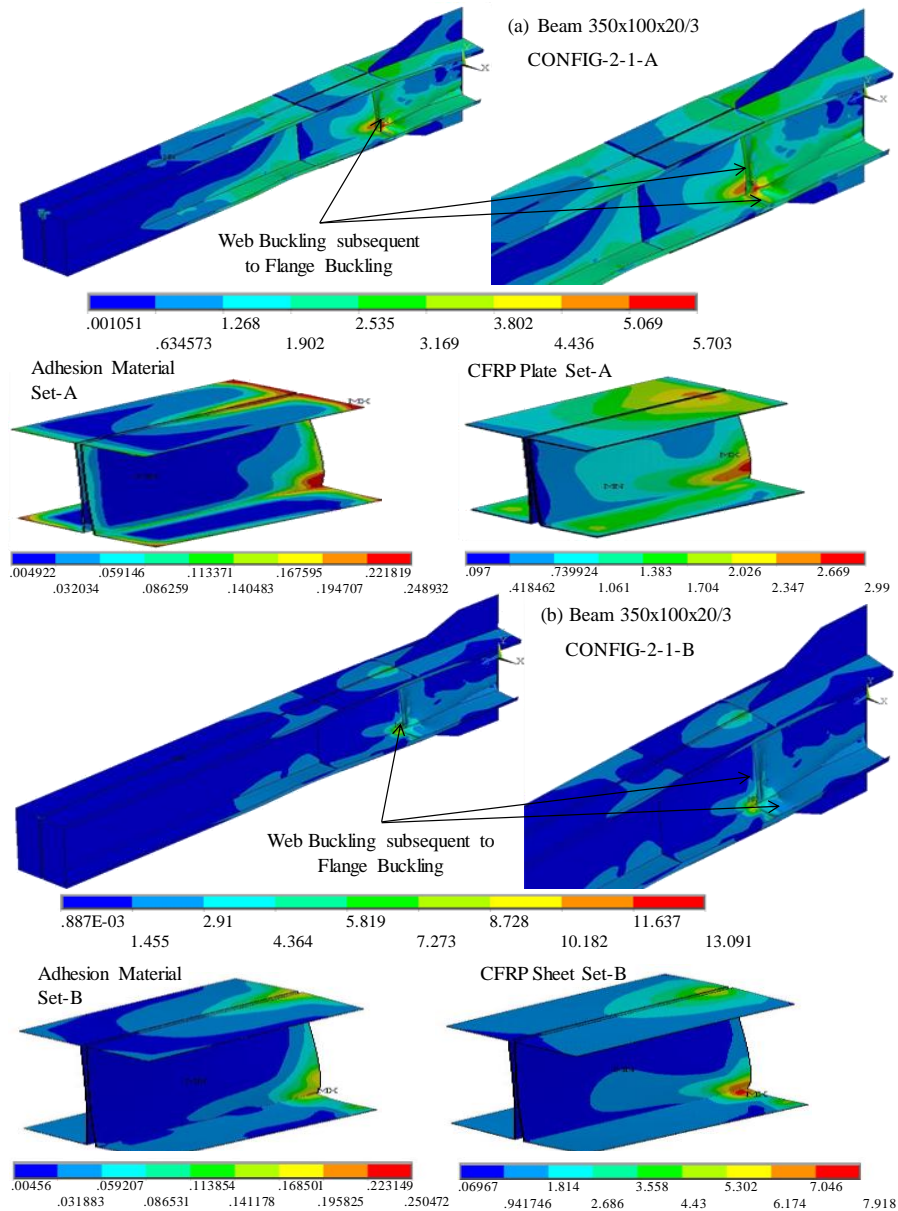


Fig. 10 Premature buckling upon utilization of CFRP strengthening: (a) CONFIG-2-1-A; and (b) CONFIG-2-1-B, with Von-Mises stress distribution in $\text{MPa} \times 10^2$

Steel Structural Systems - Special Bolted Moment Frames; American Iron and Steel Institute, Washington, D.C., USA.

ANSI/AISC 360-10 (2010), Specification for Structural Steel Buildings; American Institute of Steel Construction, IL, USA.

ANSI/AISC 341-10 (2010), Seismic Provisions for Structural Steel Buildings; American Institute of Steel Construction, IL, USA.

ANSYS release 11.0, Swanson analysis system (1998), Houston, TX, USA.

Bagheri, S.A., Petkovski, M., Pilakoutas, K. and Mirghaderi, R. (2012), "Development of cold-formed steel elements for earthquake resistant moment frame buildings", *Thin-Wall. Struct.*, **53**, 99-108.

Calderoni, B., De Martino, A., Formisano, A. and Fiorino, L. (2009), "Cold formed steel beams under monotonic and cyclic loading: Experimental investigation", *J. Constr. Steel Res.*, **65**(1), 219-227.

Casafont, M., Arnedo, A., Roure, F. and Rodriguez-Ferran, A. (2006a), "Experimental testing of joints for seismic design of

lightweight structures. Part 1. Screwed joints in straps", *Thin-Wall. Struct.*, **44**(2), 197-210.

Casafont, M., Arnedo, A., Roure, F. and Rodriguez-Ferran, A. (2006b), "Experimental testing of joints for seismic design of lightweight structures. Part 2: Bolted joints in straps", *Thin-Wall. Struct.*, **44**(6), 677-691.

Casafont, M., Arnedo, A., Roure, F. and Rodriguez-Ferran, A. (2007), "Experimental testing of joints for seismic design of lightweight structures. Part 3: Gussets, corner joints, x-braced frames", *Thin-Wall. Struct.*, **45**(7), 637-659.

Dar, M.A., Yusuf, M., Dar, A.R. and Raju, J. (2015), "Experimental study on innovative sections for cold formed steel beams", *Steel Compos. Struct., Int. J.*, **19**(6), 1599-1610.

Dinis, P.B. and Camotim, D. (2015), "Cold-formed steel columns undergoing local-distortional coupling: Behaviour and direct strength prediction against interactive failure", *Comput. Struct.*, **147**, 181-208.

Dubina, D. (2008), "Behavior and performance of cold-formed

- steel-framed houses under seismic action”, *J. Constr. Steel Res.*, **64**(7), 896-913.
- ECP-205 (ASD) (2011), Egyptian Code of Practice for Steel Construction and Bridges; Housing and Research Center, Giza, Egypt.
- El-Tawil, S., Ekin, E., Subhash, G. and Chao, S.H. (2011), “Retraining local and global buckling behavior of steel plastic hinges using CFRP”, *J. Constr. Steel Res.*, **67**(3), 261-269.
- Essam, G.S., Serror, M.H. and Ahmed, F.H. (2016), “Numerical study on the behavior of CFRP-strengthened cold-formed steel beams”, M.Sc. Thesis; Department of Structural Engineering, Faculty of Engineering, Cairo University, Egypt.
- Eurocode 3 (2005), Design of steel structures: Part 1.1: General rules and rules for buildings, EN 1993-1-1.
- Faris, A.U. and Mehtab, A. (2013), “Mechanical properties of steel-CFRP composite specimen under uniaxial tension”, *Steel Compos. Struct., Int. J.*, **15**(6), 659-677.
- Gholami, M., Mohd Sam, A.R., Marsono, A.K., Tahir, M.M. and Faridmehr, I. (2016), “Performance of steel beams strengthened with pultruded CFRP plate under various exposures”, *Steel Compos. Struct., Int. J.*, **20**(5), 999-1022.
- Gunaydin, M., Adanur, S., Altunisik, A.C. and Sevim, B. (2015), “Static and dynamic responses of Halgavor Footbridge using steel and FRP materials”, *Steel Compos. Struct., Int. J.*, **18**(1), 51-69.
- Harries, K.A., Andrew, J.P. and Elizabeth, J.A. (2009), “Enhancing stability of structural steel sections using FRP”, *Thin-Wall. Struct.*, **47**(10), 1092-1101.
- Hassan, E.M., Serror, M.H. and Mourad, S.A. (2017), “Numerical prediction of available rotation capacity of cold-formed steel beams”, *J. Constr. Steel Res.*, **128**, 84-98.
- Islam, S.M.Z. and Young, B. (2014), “FRP strengthening of lean duplex stainless steel hollow sections subjected to web crippling”, *Thin-Wall. Struct.*, **85**, 183-200.
- Lawson, R.M. (1992), “New developments in use of cold formed steel in buildings”, *Constr. Build. Mater.*, **6**(4), 201-204.
- Lim, J.B.P. and Nethercot, D. (2003), “Ultimate strength of bolted moment-connections between cold-formed steel members”, *Thin-Wall. Struct.*, **41**(11), 1019-1039.
- Linghoff, D., Haghani, R. and Al-Emrani, M. (2009), “Carbon-fiber composites for strengthening steel structures”, *Thin-Wall. Struct.*, **47**(10), 1048-1058.
- Moghimi, H. and Ronagh, H. (2009), “Performance of light-gauge cold-formed steel strap-braced stud walls subjected to cyclic loading”, *Eng. Struct.*, **31**(1), 69-83.
- Padilla-Llano, D.A., Eatherton, M.R. and Moen, C.D. (2016), “Cyclic flexural response and energy dissipation of cold-formed steel framing members”, *Thin-Wall. Struct.*, **98B**, 518-532.
- Park, J.W. and Yoo, J.H. (2015), “Flexural and compression behavior for steel structures strengthened with Carbon Fiber Reinforced Polymers (CFRPs) sheet”, *Steel Compos. Struct., Int. J.*, **19**(2), 441-465.
- Phan, D.T., Lim, J.B.P., Tanyimboh, T.T. and Sha, W. (2013), “An efficient genetic algorithm for the design optimization of cold-formed steel portal frame buildings”, *Steel Compos. Struct., Int. J.*, **15**(5), 519-538.
- Sato, A. and Uang, C-M. (2009), “Seismic design procedure development for cold-formed steel-special bolted moment frames”, *J. Constr. Steel Res.*, **65**(4), 860-868.
- Sato, A. and Uang, C-M. (2010), “Seismic performance factors for cold-formed steel special bolted moment frames”, *J. Struct. Eng.*, **36**(8), 961-967.
- Sayed-Ahmed, E.Y. (2004), “Strengthening of thin-walled steel I-section beams using CFRP strips”, *Proceedings of the 4th International Conference on Advanced Composite Materials in Bridges and Structures*, Calgary, Alberta, Canada, July.
- Serror, M.H., Hassan, E.M. and Mourad, S.A. (2016), “Experimental study on the rotation capacity of cold-formed steel beams”, *J. Constr. Steel Res.*, **121**, 216-228.
- SIKA (2016), URL: <http://usa.sika.com/en/repair-protection/02a002/02a013/02a013sa06.html>
- Silvestre, N., Young, B. and Dinar, C. (2008), “Non-linear behavior and load-carrying capacity of CFRP-strengthened lipped channel steel columns”, *Eng. Struct.*, **30**(10), 2613-2630.
- Uang, C-M., Sato, A., Hong, J-K. and Wood, K. (2010), “Cyclic testing and modeling of cold-formed steel special bolted moment frame connections”, *J. Struct. Eng.*, **136**(8), 953-960.
- Wong, M.F. and Chung, K.F. (2002), “Structural behavior of bolted moment connections in cold-formed steel beam-column sub-frames”, *J. Constr. Steel Res.*, **58**(2), 253-274.
- Yang, N., Zhong, Y., Meng, Q. and Zhang, H. (2014), “Hysteretic behaviors of cold-formed steel beam-columns with hollow rectangular section: Experimental and numerical simulations”, *Thin-Wall. Struct.*, **80**, 217-230.
- Yu, C. and Schafer, B.W. (2007), “Simulation of cold-formed steel beams in local and distortional buckling with applications to the direct strength method”, *J. Constr. Steel Res.*, **63**(5), 581-590.
- Yu, W.K., Chung, K.F. and Wong, M.F. (2005), “Analysis of bolted moment connections in cold-formed steel beam-column sub-frames”, *J. Constr. Steel Res.*, **61**(9), 1332-1352.
- Zhao, X.L. and Zhang, L. (2007) “State-of-the-art review on FRP strengthened steel structures”, *Eng. Struct.*, **29**(8), 1808-1823.
- Zhao, X.L. and Al-Mahaidi, R. (2009), “Web buckling of light steel beams strengthened with CFRP subjected to end-bearing forces”, *Thin-Wall. Struct.*, **47**(10), 1029-1036.

CC